
Article:
Ansari, S.A., Davidson, J.N. orcid.org/0000-0002-6576-3995 and Foster, M.P. orcid.org/0000-0002-8565-0541 (2021) Evaluation of silicon MOSFETs and GaN HEMTs in soft-switched and hard-switched DC-DC boost converters for domestic PV applications. IET Power Electronics, 14 (5). pp. 1032-1043. ISSN 1755-4535

https://doi.org/10.1049/pel2.12085

Received: 20 August 2020 | Revised: 10 January 2021 | Accepted: 21 January 2021

IET Power Electronics

DOI: 10.1049/pel2.12085

The Institution of Engineering and Technology WILEY

ORIGINAL RESEARCH PAPER

Evaluation of silicon MOSFETs and GaN HEMTs in soft-switched and hard-switched DC-DC boost converters for domestic PV applications

Sajad A. Ansari | **Jonathan N. Davidson** | **Martin P. Foster**

Department of Electronic and Electrical Engineering, the University of Sheffield, Sheffield, U.K.

Correspondence
Jonathan N. Davidson, Department of Electronic and Electrical Engineering, the University of Sheffield, Sheffield, U.K.
Email: Jonathan.davidson@sheffield.ac.uk

Abstract

Hard-switched high-gain DC-DC converters such as the boost converter play an important role in renewable energy systems. Research to increase their efficiency is important and can be achieved using soft-switching techniques; however, that approach requires an auxiliary circuit. The auxiliary circuit decreases power density and reliability while increasing the cost. Moreover, soft-switching topologies usually cannot improve the efficiency for all power and voltage ranges. Wide bandgap (WBG) devices, such as gallium nitride (GaN), result in lower switching losses than silicon (Si), can be used while retaining the simple structure of a hard-switched topology. However, the high cost of these devices is problematic for their frequently cost-sensitive applications. To quantify the cost and efficiency, this study compares soft-switching techniques and WBG-based switches in DC-DC boost converters for a photovoltaic (PV) energy application. The performance of four prototypes including the soft-switched and hard-switched DC-DC converters with both state-of-the-art Si and GaN switches are evaluated in terms of cost, power density, efficiency, and reliability using theoretical analysis, simulation and experimental results. It is shown that the GaN-based hard-switched converter provides higher efficiency and power density; it is more expensive than its Si-based counterpart, yet is cheaper than soft-switched converters.

1 | INTRODUCTION

Nowadays, due to the increase in energy demand and limited fossil fuel sources, research into renewable energy has increased dramatically. DC-DC converters are a significant element of renewable energy systems. For this reason, significant effort has been applied to enhance performance in recent years, with high efficiency, voltage gain, power density, dynamic response time and reliability—as well as low cost—being chief considerations [1–3].

It is well known that the volume of passive components is inversely proportional to the switching frequency. At higher switching frequencies, in addition to reduced passive component volume, a low-capacitance and low-inductance filter can be used, which also enhances the dynamic response of the system. However, increases in switching frequency are limited due to switching device availability (and cost), and also because high-frequency operation increases switching losses considerably [4]. Hence, several soft-switching techniques have been introduced to augment traditionally hard-switched DC-DC converters, thereby limiting switching losses [5–10] by commutating the devices during their zero-current or zero-voltage transitions.

However, this augmentation requires an auxiliary circuit consisting of inductors, capacitors, diodes and switches, which increases the complexity and cost of the converter [11]. In addition, the soft-switching techniques cannot provide high efficiency for all load ranges and, sometimes, they can only be used for a narrow voltage and power range. Thus, soft-switching techniques can only enhance the efficiency in the vicinity of the nominal operating conditions and for the designed applications [4]. Several authors have proposed soft-switched converters to increase efficiency for a range of applications [4–12]. There has been no rigorous analysis to confirm, once all implications of implementing a soft-switched approach have been considered,

that the solution is more meritorious than a traditional hard-switched approach. Therefore, this study compares, in terms of cost, power density, efficiency and reliability, hard- and soft-switching DC-DC converters.

The quality of the semiconductor devices has a significant influence on the performance of the DC-DC converters. Recently, significant effort has been applied to decrease the switching loss (chiefly by reducing parasitic capacitance) and conduction losses (by reducing on-state resistance) of the switching devices [13]. A breakthrough has been achieved by using wide-bandgap (WBG) materials, such as silicon carbide (SiC) and gallium nitride (GaN) [14]. The switching devices based on WBG materials can not only be switched with greater speed but also have lower switching losses compared to traditional silicon (Si) switches. In addition, they benefit from higher maximum junction temperature (if appropriately packaged) and lower conduction losses due to increased carrier mobility [15]. This allows high efficiency to be achieved at high switching frequencies with the help of WBG-based switches while the conventional simple structure of the DC-DC converter does not need to be changed.

However, the use of WBG devices has some drawbacks. First, WBG-based hard-switched converters still suffer higher switching loss than full soft-switched converters, where soft switching is applied to all commutations. Second, WBG-based switches are not yet as mature as Si switches, leading to increased cost. Furthermore, they suffer from sensitivity to parasitic components in the high-speed gate drive, high reverse-conducting voltage drop and high electromagnetic interference (EMI) because of rapid switching [16].

The superior performance of WBG-based switches over Si-based switches in terms of switching losses and switching speed has already been confirmed in the literature [17, 18]. An efficiency comparison between an Si-IGBT-based switch and a GaN-based switch in a motor drive application is provided in [19]. It is shown that the GaN-based drive has better efficiency. In [20], the efficiency of Si and SiC-based switches in a high-gain DC–DC boost converter for high-voltage low-power applications have been investigated. It was shown that the highest efficiency is obtained when the power transistor is implemented by a normally off junction field-effect transistor and the diode by a SiC Schottky device with a small parasitic capacitance. In [21], the common-mode EMI characteristics of GaN high-electron-mobility transistor (HEMT) and Si metal-oxide-semiconductor field-effect transistor (MOSFET) power converters in electric vehicle (hybrid) applications have been studied. By parametrically increasing the gate resistance of switches, the tradeoff between converter efficiency and common-mode noise generation is quantified. In [22], a comprehensive analysis has been performed between an insulated-gate bipolar transistor (IGBT) two-level converter, a SiC MOSFET two-level converter, an Si MOSFET modular multi-level converter (MMC) and a GaN HEMT MMC, in terms of power losses and cost. The five-level MMC with parallel-connected Si MOSFETs was found to be an efficient, cost-effective converter for low-voltage applications. In addition, EMI is compared between SiC and Si MMC using carefully controlled relative measurements of radiated EMI in [23]. It is shown that Si MMC offers slightly superior efficiency even with slowed switching transitions compared to a SiC two-level converter, resulting in significantly lower EMI.

Given these isolated studies, we aim to answer the important question they raise: In general, are Si-based soft-switching DC-DC converters more efficient and/or more convenient than WBG-based hard-switched DC-DC converters or is the reverse true? For completeness and to set benchmarks, we also investigate WBG-based soft-switched converters and Si-based hard-switched converters. For a comparison to be meaningful, all four options must use modern, high-performance devices. The super-junction (SJ) Si MOSFET has good performance in terms of conduction and switching losses and we, therefore, compare it to WBG-based switches.

Similar previous work has not covered the same scope. In [24], for example, the authors present a comparison of Si-based soft-switching and SiC-based hard-switching inverters. However, a comprehensive performance comparison was not presented in [24]; only cost and power losses were compared. It should be noted that the characteristics of DC-AC inverters studied in [24] and DC-DC converters studied here are significantly different. Moreover, each technique (soft-switching and state-of-the-art switches) can have different results for different applications. A method can be more efficient in a particular application such as a battery charger while it might be less suitable for another application such as in PV systems. This presents an opportunity to explore the space between hard-switched topologies with the use of soft-switching techniques, state-of-the-art SJ Si switches, and WBG semiconductors in low-voltage (< 650V) DC-DC converters for renewable energy applications comprehensively. We, therefore, present a case study that supplements existing literature and expands the scope of knowledge to encompass DC-DC converters typically used in PV applications.

In this study, the performance of four prototypes including two soft-switched and two hard-switched boost converters, each with either state-of-the-art Si MOSFETs or GaN HEMTs are investigated in terms of efficiency, power density, cost, and reliability. The topologies are based on the boost converter, which is one of the most ubiquitous step-up DC-DC converters available. It is chosen because of its simple structure and very low ripple input current, which is necessary for renewable energy applications. In addition, among renewable energy systems, modern AC-PV module (microinverter) systems have received increased attention due to their unique advantages, for example, resolving the negative influences of partial shading, higher maximum power point tracking efficiency, higher flexibility and reliability, friendly plug-and-play capability, and simple installation [25, 26]. Therefore, the performances of the aforementioned converters are compared when their characteristics in terms of voltage and power are designed to be used in microinverter applications. Hence, the results of this comparison are accurate for power levels of a few hundred watts and voltage levels of a few hundred volts. As two exemplary candidates of WBG devices, SiC MOSFETs and GaN HEMTs are regarded as the successors of Si devices in the medium-to-high-voltage (>1200 V) and low-voltage (< 650 V) domains, respectively [15]. Hence, GaN HEMT is used as WBG switch, as the voltage ranges of power switches for the designed converters are low

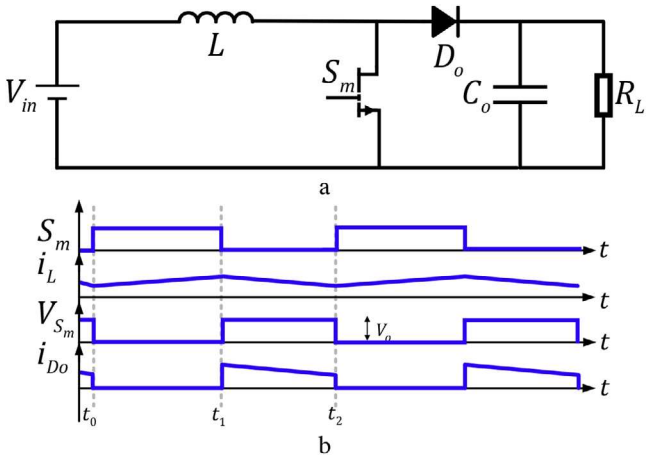

FIGURE 1 Boost converter. (a) Schematic, (b) key waveforms

in this work. All converters are investigated and then compared by the experimental and simulation results. It is shown that the GaN-based hard-switching boost converter has a better performance in terms of efficiency and power density. However, the GaN-based hard-switched converter is more expensive than its Si-based counterpart, but it is still cheaper than Si-based soft-switching converter. This is despite GaN-based switches being significantly more expensive than their Si counterparts.

This study builds on preliminary results presented at the IET power electronics, machines and drives conference, 2020, by including a more complete literature review, further simulation results and experimental validation [27]. It is organised as follows: The operating principles of hard- and soft-switched boost converters and their specifications are presented briefly in Section 2. Then, in Section 3, the four converters designs are simulated under the same operating conditions and compared in terms of efficiency, power density, reliability, and cost. Experimental validation is presented in Section 4. Finally, the discussion of achievement and a brief conclusion are given in Section 5.

2 | DC-DC CONVERTERS

2.1 | Conventional boost converter

The conventional boost converter, shown in Figure 1(a), is used as the benchmark of the study. It should be noted that the underlying principles that will be applied are ultimately generic and can be applied to a wide variety of DC-DC converter topologies.

The operation of the boost converter in continuous conduction mode (CCM) is investigated in [28], and the key waveforms over two switching periods are presented in Figure 1(b). The boost converter has two operating intervals in each switching period. In the first interval, the main switch S_m is turned on and the output diode D_o is off; thus, the boost inductor L is charged by the input source. The second interval starts when S_m is turned off and the output diode D_o turns on: The energy stored in the boost inductor is discharged to the output through diode D_o.

According to [28], the voltage gain and minimum inductance value of the boost converter in CCM operation can be calculated as Equations (1) and (2), respectively.

$$M = \frac{V_o}{V_{in}} = \frac{1}{1-D} \tag{1}$$

$$L_{min} = \frac{D(1-D)^2 V_o^2}{2 f_s P_o} \tag{2}$$

where V_{in} and V_o are input and output voltages, respectively; D is the duty ratio; f_s is the switching frequency; and P_o is the output power. The inductor peak-to-peak ripple current Δi_L can be obtained as

$$\Delta i_L = \frac{D V_{in}}{f_s L} \tag{3}$$

Similarly, peak-to-peak ripple of the output voltage can be obtained by Equation (4). In Equation (4), C_o is the output capacitance.

$$\Delta V_o = \frac{D P_o}{V_o C_o f_s} \tag{4}$$

The voltage stress (i.e. peak drain-source voltage) of the main switch is equal to the output voltage. The currents through the main switch at the start of the turn-on and turn-off events are given by Equations (5) and (6), respectively. I_{in} is the average of the input current.

$$I_{S_m(t=T_s)} = I_{in} - \Delta i_L \tag{5}$$

$$I_{S_m(t=DT_s)} = I_{in} + \Delta i_L \tag{6}$$

The root-mean-square (RMS) current of the main switch can be calculated as follows:

$$I_{S_{m.b}(rms)} = \sqrt{D I_{in}^2} \tag{7}$$

The average and RMS current of the output diode can be expressed as Equations (8) and (9), respectively.

$$I_{D_o(avg)} = I_{in}\ (1-D) \tag{8}$$

$$I_{D_o(rms)} = I_{in}\ \sqrt{(1-D)} \tag{9}$$

2.2 | Soft-switched boost converter

Table 1 presents some well-known soft-switched boost converters against which a comparison could be made. In this study, the soft-switched boost converter proposed in [6] is selected

TABLE 1 Comparison of well-known soft-switched boost converters

Ref.	Main switch		Auxiliary switch			Number of auxiliary diodes	Number of auxiliary inductors	Number of auxiliary capacitors	Number of auxiliary switches	Common ground for switches
	Turn on	Turn off	Turn on	Turn off	Conduction losses					
[5]	Soft	Soft	Soft	Soft	Low	0	1	1	1	Yes
[6]	Hard	Soft	–	–	High	5	2	2	0	–
[7]	Soft	Hard	Soft	Hard	High	0	1	1	2	No
[8]	Soft	Hard	Hard	Soft	High	3	1	1	1	Yes

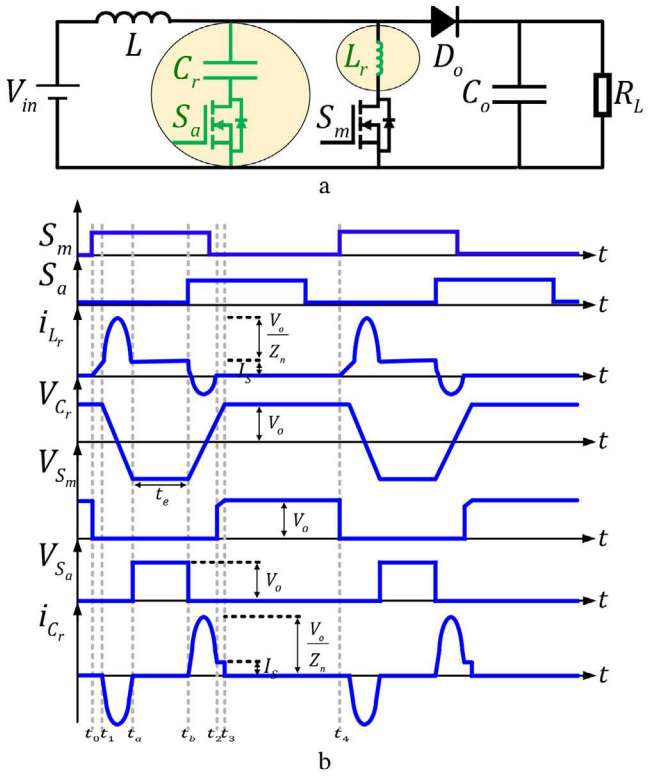

FIGURE 2 Soft-switched boost converter introduced in [5]. (a) Schematic with differences from boost converter highlighted, (b) key waveforms adapted from [5]

for analysis because, in the authors' opinion, it is well-presented and has a number of useful features. Both turn-on and turn-off are soft for both switches. In addition, the conduction losses from the auxiliary circuit are lower than its rivals. Furthermore, it requires the fewest components, suppressing complexity and cost. Its topology and key waveforms are presented in Figures 2(a) and (b), respectively.

It is worth noting that there are many other soft-switched converters based on the boost converter. However, in order for the comparison made to be fair, it is important that their circuit topology does not differ significantly from the traditional boost converter. For example, there are many high-gain (and high-order) boost converters, with and without soft-switching capability, which have plentiful applications and frequently higher efficiency as a result of lower conduction loss due to, for a given power rating, their switch currents being lower. However, such a converter is not comparable to the traditional boost converter. In this study, the comparison is made with the converter in [6] so that the only advantage achieved relates to reduced switching loss as a result of the soft switching.

The detailed operation of the chosen converter is described comprehensively in [6]; we provide only an overview in this study. As shown in Figure 2(a), auxiliary components consisting of a resonant inductor L_r, a resonant capacitor C_r, and an auxiliary switch S_a are added to the conventional structure of a boost converter.

The converter has six operation intervals. The main switch, S_m, is turned on at the zero crossing of the switch current (i.e. zero-current switched, ZCS) because it is in series with the resonant inductor L_r and it is turned off at zero crossing of the drain-source voltage (i.e. zero-voltage switched, ZVS) while the switch current flows through the antiparallel diode. The auxiliary switch, S_a, is turned on at the ZCS condition because of the presence of the resonant inductor L_r and boost inductor L, and it is turned off at the ZVS condition after the voltage of the resonant capacitor C_r reaches the output voltage.

The relationships between the voltage gain, minimum inductance value, inductor current ripple, output voltage ripple, and the average and RMS current of the output diode in this converter are similar to the relationships of the conventional boost converter. However, the RMS current of the main switch is given by Equation (10). The RMS current of the auxiliary switch and its body diode can be calculated by Equation (11); the average current of the auxiliary switch body diode alone is given by Equation (12). It is worth mentioning that the average current of the body diode of the main switch is negligible, as its current amplitude and turn-on time duration are very low:

$$I_{S_{m.sb}(rms)} \simeq \sqrt{DI_{in}^2 + \left(\frac{V_o}{2Z_n\sqrt{f_s/f_r}}\right)^2} \tag{10}$$

$$I_{S_{a.sb}(rms)} \simeq I_{D_{a.sb}(rms)} = \frac{V_o}{2Z_n\sqrt{f_s/f_r}} \tag{11}$$

$$I_{D_{a.sb}(avg)} = \frac{V_o}{\pi Z_n\sqrt{f_s/f_r}} \tag{12}$$

TABLE 2 Parameters of prototypes 1–4

Prototype	Output power	Input voltage	Output voltage	Switching frequency	Boost inductor	Resonant inductor	Output capacitor	Resonant capacitor	Switch	Diode
1	500 W	100 V	400 V	200 kHz	375 μH	–	4.7 μF	–	IPW65R150CFDA	SCS220AG
2	500 W	100 V	400 V	200 kHz	375 μH	–	4.7 μF	–	GS66506T	SCS220AG
3	500 W	100 V	400 V	200 kHz	375 μH	2 μH	4.7 μF	9.1 nF	IPW65R150CFDA	SCS220AG
4	500 W	100 V	400 V	200 kHz	375 μH	2 μH	4.7 μF	9.1 nF	GS66506T	SCS220AG

In Equations (10) to (12), Z_n is defined as $\sqrt{L_r/C_r}$, and f_r is the resonant frequency, $1/(2\pi\sqrt{L_rC_r})$. According to Equations (11) and (12), the average and RMS currents of the auxiliary components are independent of the output power. In addition, the resonant period T_r, ($= 2\pi\sqrt{L_rC_r}$) is independent of the switching frequency.

2.3 | Design characteristics of the prototypes

The conventional and soft-switched boost converters can be designed according to the methods proposed in [6, 28], and, for brevity, the design considerations of these converters are not presented in this study. Using the relationships provided in [6, 28], four prototypes including two hard-switched and two soft-switched boost topologies were designed and their specifications are presented in Table 2.

Prototypes 1 and 2 are two conventional hard-switched boost converters, while prototypes 3 and 4 are soft-switched boost converters. Meanwhile, prototypes 1 and 3 use Si SJ MOSFETs, while prototypes 2 and 4 use GaN HEMTs. All prototypes use a state-of-the-art low-loss SiC Schottky diode for D_o. To the extent possible, the rated voltage and current of all devices are similar, and each device is state-of-the-art in its category to provide a realistic comparison.

3 | COMPARISON

In this section, the prototypes are compared and evaluated in terms of efficiency, power density, reliability and cost using simulation results and theoretical analysis.

3.1 | Power loss analysis

The relationship in Equation (13) is used for efficiency calculation. The losses of the components are obtained based on the losses calculation procedure presented in [29, 30]:

$$\eta = \frac{P_o}{P_o + P_{Loss}} \tag{13}$$

In considering the power losses of each converter, the switching losses ($\sum P^S_{Loss}$), diode losses ($\sum P^D_{Loss}$), capacitor losses ($\sum P^C_{Loss}$), and inductor losses ($\sum P^L_{Loss}$) are considered. The power losses of a converter can be obtained by Equation (14):

$$P_{Loss} = \sum P^S_{Loss} + \sum P^D_{Loss} + \sum P^C_{Loss} + \sum P^L_{Loss} \tag{14}$$

The losses from the diodes can be obtained from Equation (15), where V_f and R_D are the forward voltage drop and series resistances of the diodes, respectively. $I_{D(avg)}$ and $I_{D(rms)}$ are average and RMS currents of the diodes, respectively. To simplify the analysis, reverse recovery losses associated with D_o are neglected, as they have a negligible influence on the power losses when a SiC Schottky diode is used [31]:

$$P^D_{Loss} = R_D\, I^2_{D(rms)} + V_f I_{D(avg)} \tag{15}$$

The power losses of the switches (P^S_{Loss}) can be calculated by Equation (16):

$$P^S_{Loss} = P^{S,switching}_{Loss} + P^{S,conduction}_{Loss} + P^{S,gate}_{Loss} \tag{16}$$

The power losses of the switches include three terms. The first term is switching losses, which can be calculated from Equation (17). In this equation, t_{on} is the current rise time plus voltage fall time, and t_{off} is the current fall time plus voltage rise time:

$$P^{S,switching}_{Loss} = \frac{1}{2}\Delta V_{DS}(I_{S_m(t=T_s)}t_{on} + I_{S_m(t=DT_s)}t_{off})f_s \tag{17}$$

The second term is the conduction losses. These losses occur in the switch channel when the current is positive, and in the body diode when the current is negative. The conduction losses of switches can be calculated as Equation (18):

$$P^{S,conduction}_{Loss} = R_{ds(on)}\, I^2_{D(rms,i_D>0)} + P^D_{Loss(i_D<0)} \tag{18}$$

where $R_{ds(on)}$ is the on-state resistance of the power switches, $I_{D(rms,i_D>0)}$ is the RMS current of the power switch when the drain current is positive, and $P^D_{Loss(i_D<0)}$ is losses of its antiparallel diode when drain current is negative.

The third term is the gate drive losses, which depends on total input gate charge of the switch Q_g, switching frequency f_s, and the voltage applied to the gate driver V_{gg} and can be calculated

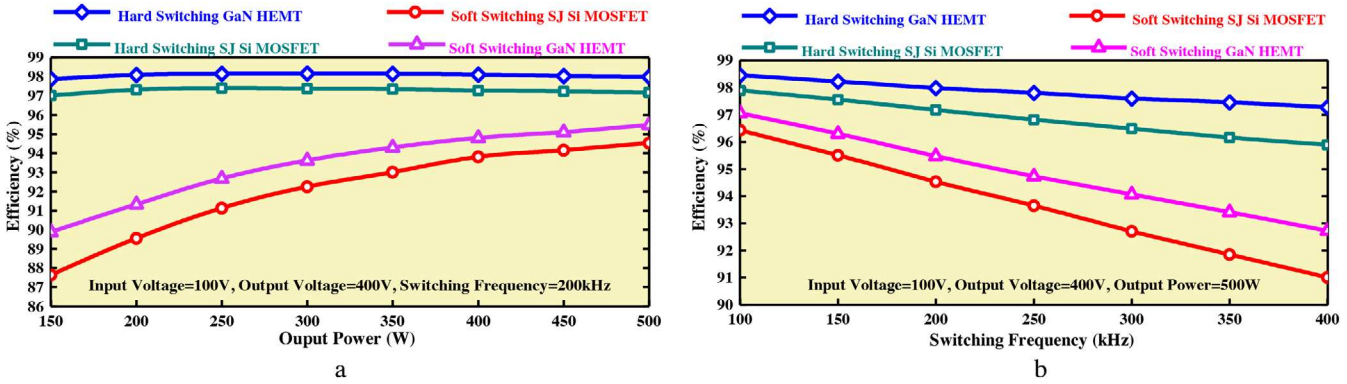

FIGURE 3 Efficiency comparison. (a) For different output powers, (b) for different switching frequencies at nominal specifications. Case temperature $T_c = 25°C$, $r_{Co} = 15\ m\Omega$, $r_{Cr} = 15\ m\Omega$, powder core (T157-8), $r_L = 60\ m\Omega$, $\Delta i_L = 1A$, $r_{Lr} = 10\ m\Omega$

according to Equation (19):

$$P_{\text{Loss}}^{S,\text{gate}} = f_s\, V_{gg} Q_g \tag{19}$$

The losses of the capacitors due to their equivalent series resistances (r_C) can be calculated by the following relationship where $I_{C(\text{rms})}$ is the RMS current through the capacitor:

$$P_{\text{Loss}}^{C} = r_C\, I_{C(\text{rms})}^2 \tag{20}$$

Losses in the inductors result from ohmic ($P_{\text{Loss}}^{L,\text{ ohmic}}$) and core losses. The ohmic losses of the inductors can be calculated as Equation (21):

$$P_{\text{Loss}}^{L,\text{ ohmic}} = r_L\, I_{L(\text{rms})}^2 \tag{21}$$

where $I_{L(\text{rms})}$ is the RMS current of the inductor and r_L is the equivalent series resistance of the inductor. Inductors also suffer eddy-current and hysteresis loss, which depend on the type of core and ripple of flux density and can be calculated from the datasheet.

The simulated efficiency curves for each of the considered topologies are shown versus output power and switching frequency in Figures 3(a) and (b), respectively. To obtain the losses accurately, all designed converters have been simulated in similar operating conditions indicated in Table 2. Since inductor design has a large influence on cost, volume and efficiency, the inductor was optimised for each switching frequency. Each design uses a powder core; the design process and core selection were performed using the procedure laid out in [32], and the closest commercially available option was chosen. For the auxiliary inductor, which suffers much higher losses, an inductor with approximately 50% outer diameter was chosen.

The power losses and efficiencies are calculated for each data point using data provided in the components' datasheets. As shown in Figure 3(a), prototype 2, the hard-switched boost converter in which the GaN HEMT switch was used, provides the highest efficiency, while prototype 1, the SJ Si-based hard-switched boost converter, is ranked second. However, the soft-switched boost converters (prototypes 4 and 3), which are based on GaN HEMT and SJ Si MOSFET, are surprisingly ranked third and fourth, respectively.

Since prototype 4 uses GaN switches with lower on-resistance, it has better efficiency, compared to prototype 3. To explain the reason, perhaps counterintuitively, the efficiency of the hard-switched boost converter is higher than its soft-switched equivalent even though both use similar semiconductors, we consider the following:

1. In high-gain and high-power DC-DC converters, conduction losses are usually the dominant losses. Therefore, in this case, since the power and input current of the converters are large, the influence of the switching losses is lower than the conduction losses.
2. The higher the input current, the more the conduction losses in the auxiliary components. Hence, even though this soft-switched converter has low conduction losses at low power, its conduction losses at high gain and high power are higher than a comparable hard-switched converter.
3. There is a resonant inductor in the auxiliary circuit that suffers significant core loss at high frequency and high current ripple.

It is worth noting that the parasitic capacitances of the high-voltage-rated (>400 V) switches and diodes are about 10 times higher under very low drain-source voltage (<10 V). Therefore, in soft-switched converters in which switches and diodes are switched under ZVS conditions, the parasitic capacitances are high, in the nanofarad range. The parasitic capacitances of the semiconductors, printed circuit board (PCB) tracks and passive components usually cause high-frequency voltage oscillation across the semiconductor devices of the converter. In very low voltage converters (<50 V), the amplitude of this oscillation is also low; however, it becomes significant at high voltage, which increases the losses of the converter, especially core losses.

To show the effect of high parasitic capacitance on the operation of the converter, the simulation results for the voltage and current of the switches in the soft-switched converter when the components are ideal and non-ideal are shown in Figures 4

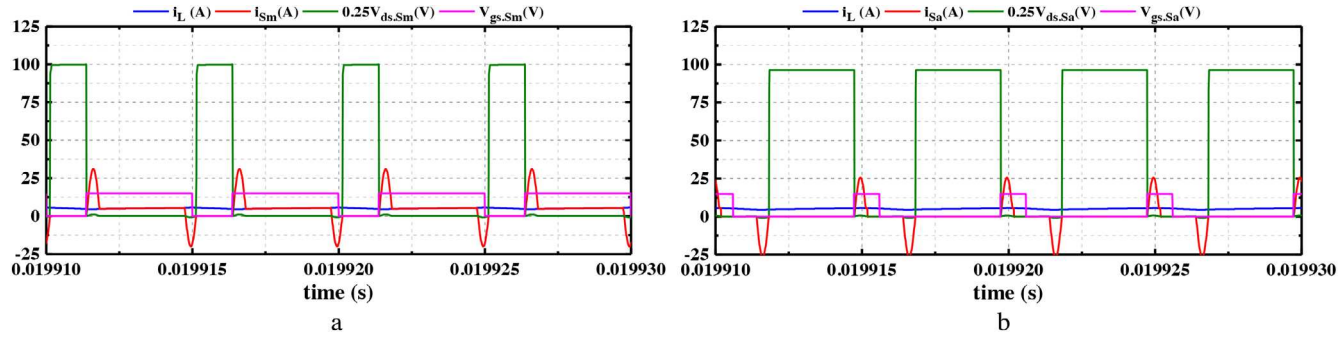

FIGURE 4 Simulation results of the ideal soft-switched boost converter. (a) i_L, i_{Sm}, $V_{ds.Sm}$, $V_{gs.Sm}$; (b) i_L, i_{Sa}, $V_{ds.Sa}$, $V_{gs.Sa}$

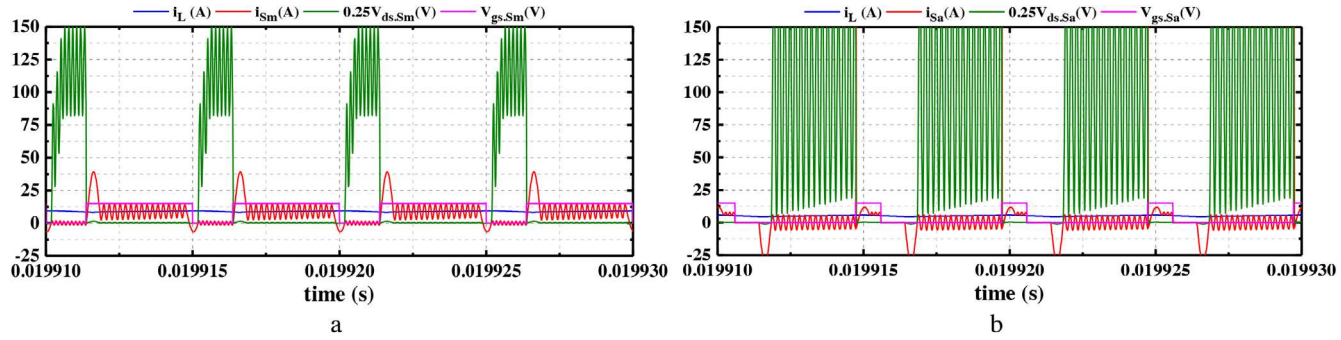

FIGURE 5 Simulation results of the non-ideal soft-switched boost converter. (a) i_L, i_{Sm}, $V_{ds.Sm}$, $V_{gs.Sm}$; (b) i_L, i_{Sa}, $V_{ds.Sa}$, $V_{gs.Sa}$

and 5, respectively. As shown in these figures, the parasitic elements have a noticeable influence on the circuit operation and hence efficiency in the high power and voltage ranges.

According to Equations (11) and (12), since the resonant current is relatively load-independent and its losses are near-constant from low power to high power, the efficiency of the soft-switched converter decreases at light power. Hence, the soft-switched topology can only provide high efficiency at nominal load condition. Accordingly, in PV systems and other applications where the input or load variation is considerable and operation is far away from the nominal design, boost converters featuring auxiliary circuits have reduced suitability due to the detrimental effects of currents circulating in their auxiliary branch.

The efficiency of the GaN-based hard-switched converter (prototype 2) is higher than SJ Si-based hard-switched converter (prototype 1), as not only the GaN switch has lower switching losses, but the switch also benefits from lower conduction losses due to lower on-state resistance. Since the GaN-based hard-switched converter does not have any auxiliary circuits, its efficiency does not decrease at low powers but actually increases due to lower conduction losses. Hence, this converter is suitable for renewable energy applications such as AC-PV module systems.

In Figure 3(b), the simulated efficiency of each considered topology operated at different switching frequencies at nominal specifications is presented. The efficiency of the hard-switched topologies decreases with higher switching frequency as expected. In addition, because the GaN-based switches have a reduced switching loss, compared to Si-based switches, the difference in efficiency between GaN-based and Si-based hard-switched converters increases as the switching frequency increases. For example, at 100 kHz, the difference is 0.5%, while it is 1% at 400 kHz.

One might predict that the influence of switching frequency is lower for soft-switched converters. However, for the aforementioned reasons, the dominant losses in microinverter applications are conduction losses; since the resonant period is frequency-independent and does not decrease with switching period, the conduction losses in the auxiliary components increase at higher switching frequency. In addition, the core loss of the resonant inductor increases noticeably as the switching frequency increases.

The loss distributions of the all prototypes at nominal specifications are illustrated in Figure 6. It can be observed that the Si-based hard-switched converters have the highest switching losses; the switching losses of the soft-switched converters are negligible. However, the soft-switched converters suffer from higher conduction and core losses, as they have an auxiliary switch, capacitor, and inductor. In spite of the low value of the resonant inductor, it has high core losses, as it is in series with the main switch, which causes a high current ripple in it.

Although the soft-switched converter has lower switching losses than a hard-switched converter, which uses a state-of-the-art power switch, it has lower efficiency and cannot provide high efficiency for light load ranges. Therefore, on efficiency alone,

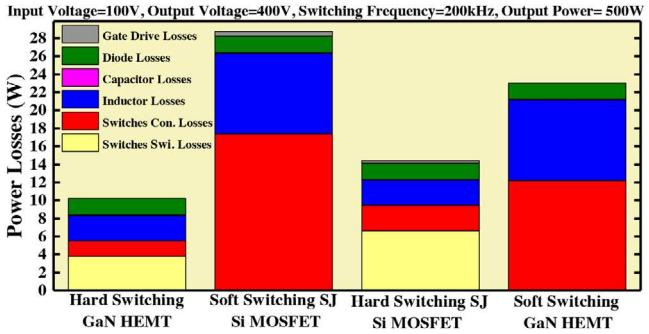

FIGURE 6 Loss distribution of the converters. $T_c = 25°C$, $r_{Co} = 15\ m\Omega$, $r_{Cr} = 15\ m\Omega$, powder core (T157-8), $r_L = 60\ m\Omega$, $\Delta i_L = 1A$, $r_{Lr} = 10\ m\Omega$

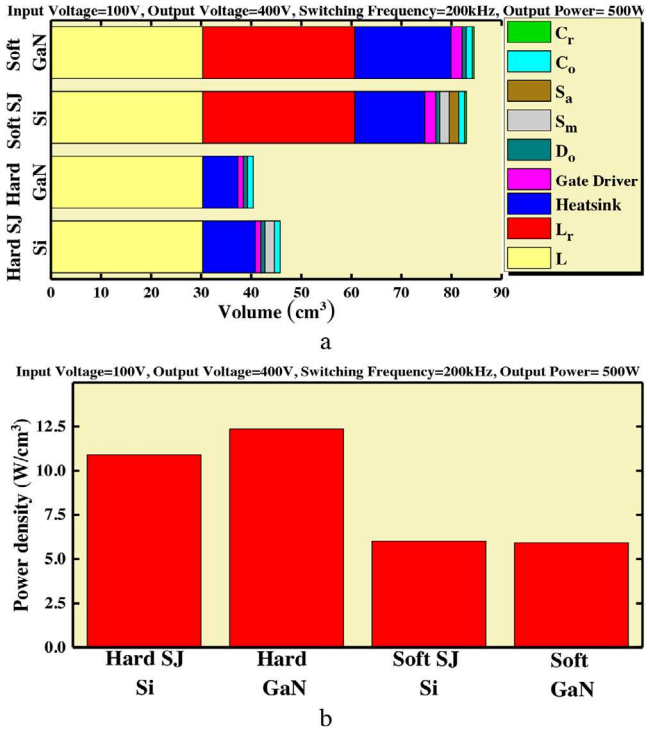

FIGURE 7 Comparison between all prototypes. (a) Volume, (b) power density. $L = L_r$ = T157-8, C_o = KEMET ESH475M450AH2AA, C_r = WIMA FKP2J014701I00HSSD

the GaN-based hard-switched converter is a better choice for AC-PV module applications.

3.2 | Power density analysis

In this section, the volume of the components used in the implementation of the converters, including capacitors, inductors, switches, diodes, gate drivers and heatsinks are compared. In order to simplify the analysis, the volume of the control system and PCB layout is not considered.

In order to provide a fair comparison, the design power of each of the converters is 500 W. The volumes, which will be presented in Figure 7(a), are, therefore, inversely proportional to the power density and are themselves an indication of performance.

The following relationship is used to calculate the minimum thermal resistance R_{Sa} of the required heatsink for each device:

$$R_{sa} = \left[\frac{T_j - T_a}{P_d} - R_{jc} - R_{cs}\right] \tag{22}$$

where, P_d represents the losses of the device, T_a is the ambient temperature (assumed in this work to be 25°C), T_j is junction temperature, R_{jc} is junction-to-case thermal resistance, and R_{cs} is the case-to-heatsink thermal resistance. In cases where no heatsink is required, the junction temperature of the device can be calculated from Equation (23).

$$T_j = P_d\ R_{ja} + T_a \tag{23}$$

In this equation, R_{ja} is the junction-to-ambient thermal resistance. Assuming the use of SIL PAD TSP 1800ST insulating pad [33], the case-to-heatsink thermal resistance R_{cs} for the output diode, GaN HEMT and SJ Si MOSFET are 1.6, 8.6, and 0.57 W/°C, respectively. Note that, since the GaN HEMT switch has the smallest contact area, its case-to-heatsink thermal resistance is the biggest. The losses of the output diode in all prototypes at nominal specifications are around 1.8 W; therefore, according to Equation (23), the output diode does not require a heatsink. However, it might need a heatsink in higher power ranges ($P_o > 500W$). The values of R_{jc} and T_j for all semiconductors are given in their datasheets. The power losses of the main switch in the Si MOSFET-based and GaN HEMT-based hard-switched boost converters at nominal specifications are 9.4 and 5.5 W, respectively. According to Equation (22), the main switches of GaN-based and Si-based hard-switched topologies each need a heatsink with R_{sa} lower than 13.4 and 11 W/°C, respectively. Therefore, the Fischer Electronic SK 55275AL and SK 55250AL heatsinks are selected for the main switches of the prototypes 1 and 2, respectively. In prototype 3, the losses of the main and auxiliary switches at nominal conditions are about 10.6 and 6.8 W, respectively. Hence, the Fischer Electronic SK 55275AL and SK 55225AL heatsinks are selected for the main and auxiliary switches, respectively, since the main and auxiliary switches need a heatsink with R_{sa} lower than 9.5 and 16.4 W/°C, respectively. Finally, the losses of the main and auxiliary switches in prototype 4 are 6.9 and 5.3 W, respectively. Since the main and auxiliary switches need a heatsink with R_{sa} lower than 8.8 and 14.3 W/°C, respectively, the Fischer Electronic SK 552100AL and SK 55237.5AL heatsinks are selected for the main and auxiliary switches, respectively.

The volume and power density of all the converters are compared in Figures 7(a) and (b), respectively. Soft-switched boost converters have larger volume. The volume of their control system and PCB layout are larger; however, even without considering them, the hard-switched converters still have lower volume than the soft-switched topologies. As shown in Figure 7(a), the

TABLE 3 Component costs

Component	Cost (£)	Supplier
IPW65R150CFDA	4.25	Mouser Electronics [32]
GS66506T	14.85	Mouser Electronics [32]
SCS220AG	7.86	Mouser Electronics [32]
WIMA FKP2J014701I00HSSD	0.47	Mouser Electronics [32]
SI8261BAC-C-IP	2.10	Mouser Electronics [32]
KEMET ESH475M450AH2AA	0.43	Mouser Electronics [32]
SK 55225AL	0.26	Anglialive [33]
SK 55250AL	0.42	Anglialive [33]
SK 55275AL	0.45	Anglialive [33]
SK 552100AL	0.49	Anglialive [33]
SK 55237.5AL	0.28	Anglialive [33]
T-157-8	6.5	Pace Components [34]

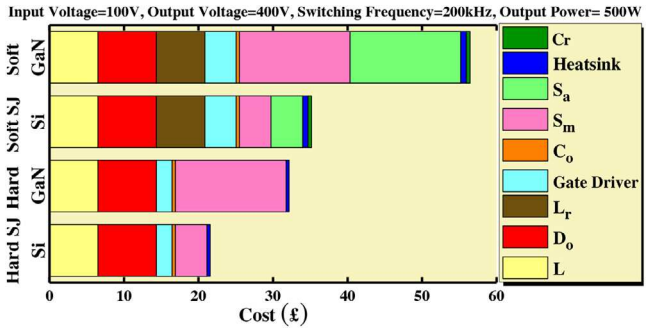

FIGURE 8 Cost comparison for all prototypes

GaN-based hard-switched converter (prototype 2) is the smallest converter. Despite the higher case-to-heatsink thermal resistance of the GaN HEMT, compared to the SJ Si MOSFET, it requires a smaller heatsink, as it has far lower losses. However, in the soft-switched prototypes, the GaN-based topology (prototype 4) needs a larger heatsink than the Si-based topology (prototype 3) because the difference between the switches losses is small.

The GaN HEMT-based hard-switched boost converter, thus, has a better power density than the SJ Si MOSFET-based soft switching boost converter. It is, therefore, a better choice for AC-PV module applications in which a DC-DC converter is needed for each PV module.

3.3 | Cost analysis

In this section, the costs of all the prototypes are evaluated based on the average price of their components in the main international distributors of electronic components [34–36].

According to the components used in power density subsection, the cost of all components and converters are presented in Table 3 and Figure 8, respectively. It has to be mentioned that this analysis is provided in January 2020, and these prices may vary across days. Power switches, capacitors, inductors, gate drivers, heatsinks, and diodes are considered, and to simplify the analysis, the cost of PCB, inductor winding and control system are neglected. As shown in Figure 8, the GaN HEMT-based hard-switched converter (prototype 2) is £10.57 more expensive than SJ Si MOSFET-based hard-switched converter (prototype 1). However, even though GaN switches are far more expensive than SJ Si switches, the GaN HEMT-based hard-switched converter is still cheaper than the soft-switched converters (£3 cheaper than prototype 3 and £24 cheaper than prototype 4). It is worth noting that the technology of Si and GaN switches are not equally mature, and this cost gap may close in the future. The cost of the control system and PCB layout for the soft-switched converter is likely higher than for the hard-switched converter, but even neglecting this, the cost of the GaN-based hard-switched converter is lower than the soft-switched topologies. The GaN-based hard-switched topology is, therefore, a better choice for renewable energy applications like AC-PV module systems in which cost is critically important. However, considering cost alone, the hard-switched topology, which uses SJ Si switches, is the best choice since it has the lowest cost presently.

3.4 | Final remarks

Increasing turn-on and turn-off time (e.g. by changing the gate resistance) for both Si and GaN switches enhances their reliability since it helps to diminish the voltage overshoot of the switches due to parasitic inductances and capacitances in the circuit. However, it also increases the switching losses. Fortunately, this capability can be used in the selected soft-switched boost converter topologies, as it does not have a significant influence on switching losses. Even though GaN switches benefit from fast switching, they suffer from high gate-drive complexity and risk of oscillation, both of which affect the reliability. Mean time to failure for a Si MOSFET switch is about 1.5×10^8 h, while for GaN it is approximately 1.9×10^6 h [22]; thus, the GaN power devices are presently significantly less reliable.

According to the aforementioned results, it is clear that the GaN HEMT-based hard-switched converter has a better performance in terms of efficiency and power density, compared to Si SJ MOSFET-based hard-switched topology and soft-switching topologies. However, this converter is more expensive than Si SJ MOSFET-based hard-switching topology but is less costly than soft-switched topology.

As we have seen, GaN switches have lower reliability, compared to their Si counterpart. In addition and in general, soft-switched boost converters, which have more components and a complicated control system, have reduced reliability. The decision on which topology to use for any application must take into account these considerations.

Finally, the results of this comparison are accurate for power levels of a few hundred watts and voltage levels of a few hundred volts, which are typical in renewable energy applications like AC-PV module systems. Extension to other scenarios such as very

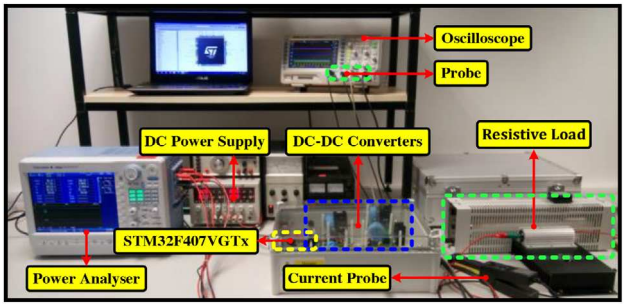

FIGURE 9 Experimental set-up

low voltage and power applications is beyond the scope of this study.

4 | EXPERIMENTAL RESULTS

In order to confirm the theoretical analysis and simulation results, all four prototypes were implemented and compared using experimental results. The laboratory set-up is shown in Figure 9. The DC link voltage is kept constant at 100 V by a DC power supply, and a power analyser (Yokogawa PX8000) is used to measure the efficiency of the converters. An advanced RISC machines (ARM)-based microcontroller STM32F407VGTx discovery board is used to generate the gating pulses with an appropriate duty ratio for the switches of the converters. The load includes a constant resistance (150 Ω) in series with a rheostat that can be changed from 10 to 1000 Ω to adjust the output power of the converters.

To maximise the performance of the converters, some of the design techniques implemented in this set-up are presented as follows. First of all, the earth tracks are placed immediately below the supply tracks on the PCB to decrease the stray magnetic flux and reduce EMI because of leakage inductance. Second, small film capacitors (1 μF) are placed near the switches to create a low impedance path for the switching signals, and the gate drivers are placed as close as possible to their switches. Third, the effects due to stray electric and magnetic fields are reduced by minimising the length of tracks. In addition, the heatsink is connected to the underside of PCB such that it does not act as a voltage-driven antenna. Finally, the initial temperature of the heatsink is 25°C.

The output voltage, V_o, the drain-source voltage, $V_{ds.Sm}$, drain current, i_{Sm} and gate-source voltage of the main switch, $V_{gs.Sm}$ in Si-based and GaN-based hard-switched boost converters are shown in Figures 10(a) and (b), respectively. The switching frequency is 200 kHz, the output power is 500 W, and the output and input voltages are 400 and 100 V, respectively. The main switches of the both converters are turned on and off at the hard switching condition, which causes switching losses. Also, the output voltage, V_o, the drain-source voltage, $V_{ds.Sm}$, drain current, i_{Sm}, and gate-source voltage of the main switch, $V_{gs.Sm}$ in Si-based and GaN-based soft-switched boost converters are illustrated in Figures 11(a) and (b), respectively. As shown in Figures 11(a) and (b), the operation of the soft-switched and hard-switched boost converters are the same in general, as the boost inductor is charged by the input source and then discharges to the output. In addition, it can be seen that, in prototypes 3 and 4, the switches are switched at soft-switching conditions (they are turned on at ZCS condition and turned off at ZVS condition), which makes their switching losses negligible. In addition, as predicted in Section 3, the parasitic components cause a high-frequency oscillation in the circuits, especially for ZVS topologies. The efficiency of all prototypes versus output power and switching frequency are measured and compared in Figures 12(a) and (b), respectively. In addition, the predicted efficiency of the prototypes calculated by the simulation results is shown with a dotted line in Figures 12(a) and (b). The experimental results confirm the efficiency comparison provided in Figure 3. The difference between the measured efficiency and the theoretical prediction ranges from 1% in the hard-switched topologies to about 3% in the soft-switched topologies.

There are a number of factors that explain these discrepancies. First, the parasitic resistances, capacitances and inductances in the layout paths were not considered in the theoretical analysis. Second, the variable nature of the switching frequency, whose experimental value is sensitive to unmodelled parasitic elements, does not result precisely in the expected theoretical value. The component characteristics, sourced from the datasheets and used for theoretical analysis, are subject to tolerance and voltage and temperature dependencies. Moreover, even though the switching losses are neglected in the soft-switched topologies, they are not eliminated completely. Furthermore, as mentioned in Section 2, the parasitic capacitors have an important influence on the operation of the soft-switched converter, especially conduction and core losses.

However, even considering these discrepancies, the experimental results still confirm the predicted efficiencies provided in Section 3. As predicted in the theoretical analysis, the GaN-based hard-switched boost converters are the most efficient, while the Si-based soft-switched boost converter has the lowest efficiency. In addition, the Si-based hard-switched and GaN-based soft-switched converters are ranked second and third, respectively. All the aforementioned explanations for Figure 3 provided in Section 3.1 remain valid for Figure 12, so are not repeated here.

The power density and cost comparison provided in Section 3 are based on the experimental results and are not subject to experimental validation, as datasheet dimensions and price-list values are not prone to experimental variation.

5 | DISCUSSION AND CONCLUSION

In this study, to investigate various methods used to decrease the switching losses of the DC-DC converters, four prototypes are implemented and evaluated. These were: (1) A hard-switched DC-DC boost converter that uses a state-of-the-art SJ Si MOSFET; (2) a version of prototype 1 using a GaN HEMT power switch; (3) a fully soft-switched DC-DC boost converter based on SJ Si MOSFET; and (4) a GaN HEMT version of prototype 3. All the prototypes were simulated and tested experimentally under the same operating conditions to compare their efficiency,

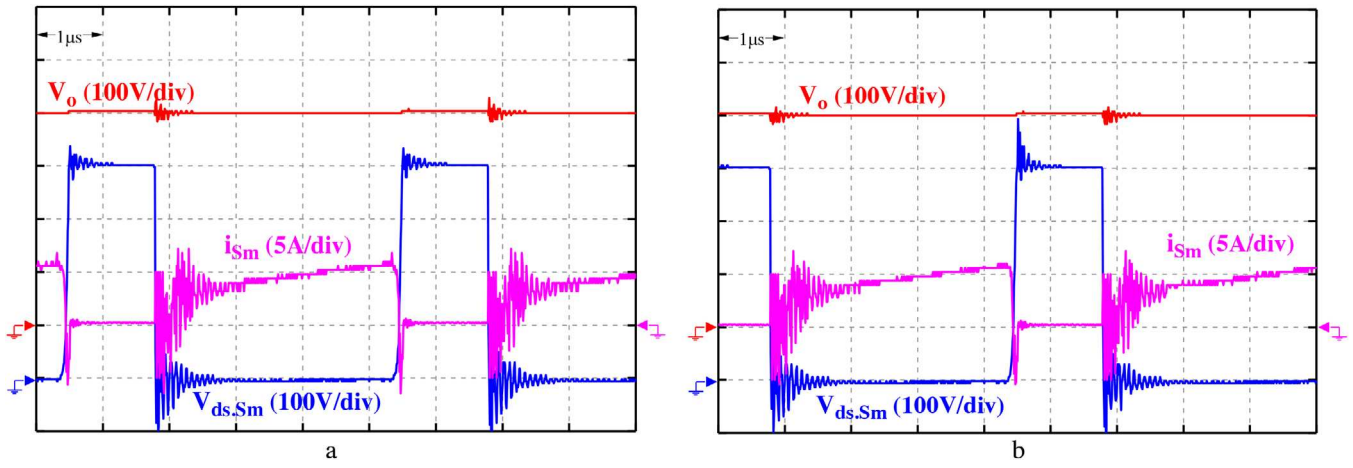

FIGURE 10 Experimental results. V_o, $V_{ds.S_m}$, $V_{gs.Sm}$, and i_{S_m} in (a) prototype 1, (b) prototype 2

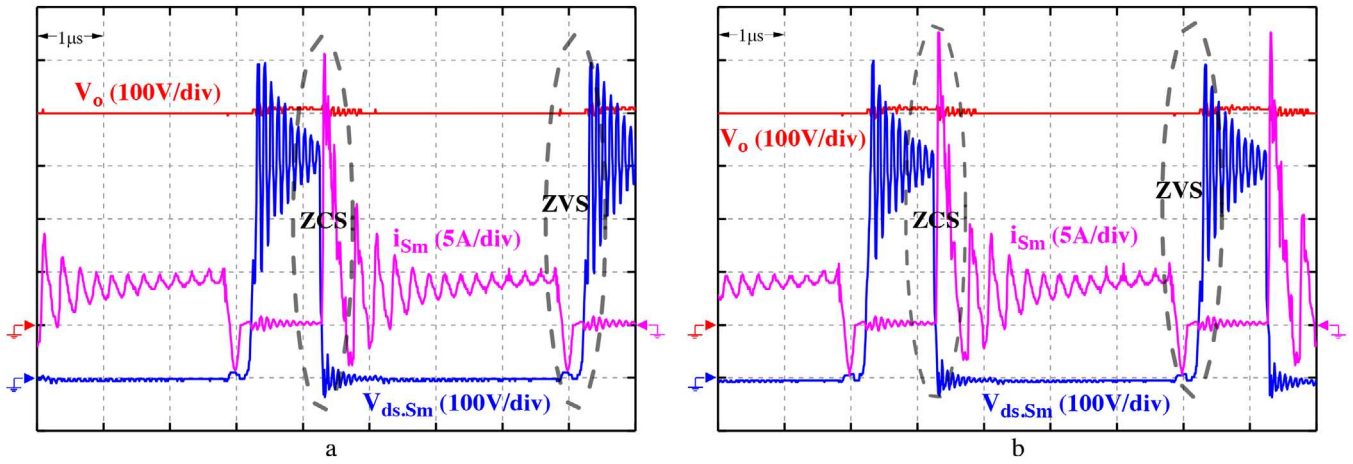

FIGURE 11 Experimental results. V_o, $V_{ds.S_m}$, $V_{gs.Sm}$, and i_{S_m} in (a) prototype 3, (b) prototype 4

power density and cost when they are designed to be used in renewable energy applications such as AC-PV module systems.

The GaN-based hard-switched converter can provide the highest efficiency from light power (100 W) to nominal power (500 W) range, and Si-based hard-switched converter is ranked second. However, the GaN-based and Si-based soft-switched converters hold the third and fourth rank, respectively. In addition, the efficiency of the soft-switched converters decreases

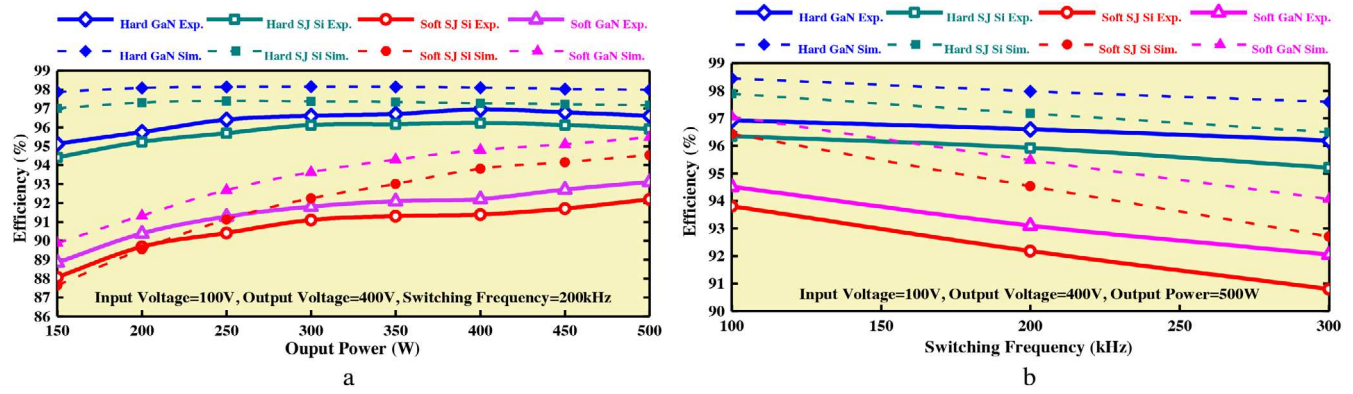

FIGURE 12 Experimental efficiency comparison. (a) For different output powers, (b) for different switching frequencies at nominal specifications

noticeably at light power range; thus, they are not a good choice for PV systems in which power range varies across hours and seasons. Furthermore, it is shown that the GaN-based hard-switched converter occupies the smallest volume.

The Si-based hard switching is the cheapest converter, and the GaN-based hard switching converter is ranked second. However, the GaN-based hard-switched converter remains cheaper than Si-based soft-switched converter, even though GaN switches are far more expensive than Si switches. In addition, this cost gap between Si and GaN switches may close in the future. Overall, using GaN in DC-DC converter does not alter the simple traditional, it has a simple structure of the converter and has better performance in terms of power density, cost, and efficiency than the soft-switched converter, and it is a better choice for renewable energy applications.

ORCID

Sajad A. Ansari https://orcid.org/0000-0003-2293-0009
Jonathan N. Davidson https://orcid.org/0000-0002-6576-3995

REFERENCES

1. Ansari, S.A., Moghani, J.S.: A novel high voltage gain non-coupled inductor SEPIC converter. IEEE Trans. Ind. Electron. 66(9), 7099–7108 (2019)
2. Ansari, S.A., et al.: A new high step-up gain SEPIC converter for renewable energy applications. In: 2019 10th International Power Electronics, Drive Systems and Technologies Conference (PEDSTC), Shiraz, Iran, pp. 539–544 (2019)
3. Mirzaee, A., Arab Ansari, S., Shokrollahi Moghani, J.: Single switch quadratic boost converter with continuous input current for high voltage applications. Int. J. Circuit Theory Appl. 48(4), 587–602 (2020)
4. Ansari, S.A., Moghani, J.: Soft switching flyback inverter for photovoltaic AC module applications. IET Renewable Power Gener. 13(13), 2347–2355 (2019)
5. Smith, K.M., Smedley, K.M.: A comparison of voltage-mode soft-switching methods for PWM converters. IEEE Trans. Power Electron. 12(2), 376–386 (1997)
6. Hui, S., Cheng, K.E., Prakash, S.N.: A fully soft-switched extended-period quasi-resonant power-factor-correction circuit. IEEE Trans. Power Electron. 12(5), 922–930 (1997)
7. Fujiwara, K., Nomura, H.: A novel lossless passive snubber for soft-switching boost-type converters. IEEE Trans. Power Electron. 14(6), 1065–1069 (1999)
8. Gurunathan, R., Bhat, A.K.: A zero-voltage transition boost converter using a zero-voltage switching auxiliary circuit. IEEE Trans. Power Electron. 17(5), 658–668 (2002)
9. Streit, R., Tollik, D.: High efficiency telecom rectifier using a novel soft-switched boost-based input current shaper. In: Thirteenth International Telecommunications Energy Conference-INTELEC 91, Kyoto, Japan, pp. 720–726 (1991)
10. Liu, K.-H., Oruganti, R., Lee, F.C.: Resonant switches–Topologies and characteristics. In: 1985 IEEE Power Electronics Specialists Conference, Toulouse, France, pp. 106–116 (1985)
11. Arab Ansari, S., Moghani, J.S., Mohammadi, M.: Analysis and implementation of a new zero current switching flyback inverter. Int. J. Circuit Theory Appl. 47(1), 103–132 (2019)
12. Yao, T., Nan, C., Ayyanar, R.: A new soft-switching topology for switched inductor high gain boost. IEEE Trans. Ind. Appl. 54(3), 2449–2458 (2018)
13. Millán, J., et al.: A survey of wide bandgap power semiconductor devices. IEEE Trans. Power Electron. 29(5), 2155–2163 (2013)
14. Jones, E.A., Wang, F.F., Costinett, D.: Review of commercial GaN power devices and GaN-based converter design challenges. IEEE J. Emerging Sel. Top. Power Electron. 4(3), 707–719 (2016)
15. Taylor, A., et al.: Comparison of SiC MOSFET-based and GaN HEMT-based high-efficiency high-power-density 7.2 kW EV battery chargers. IET Power Electron. 11(11), 1849–1857 (2018)
16. Liu, B., et al.: Impacts of high frequency, high di/dt, dv/dt environment on sensing quality of GaN based converters and their mitigation. CPSS Trans. Power Electron. Appl. 3(4), 301–312 (2018)
17. Mitova, R., et al.: Investigations of 600-V GaN HEMT and GaN diode for power converter applications. IEEE Trans. Power Electron. 29(5), 2441–2452 (2013)
18. Zhao, B., Song, Q., Liu, W.: Experimental comparison of isolated bidirectional DC–DC converters based on all-Si and all-SiC power devices for next-generation power conversion application. IEEE Trans. Ind. Electron. 61(3), 1389–1393 (2013)
19. Shirabe, K., et al.: Efficiency comparison between Si-IGBT-based drive and GaN-based drive. IEEE Trans. Ind. Appl. 50(1), 566–572 (2013)
20. León-Masich, A., et al.: Efficiency comparison between Si and SiC-based implementations in a high gain DC–DC boost converter. IET Power Electron. 8(6), 869–878 (2015)
21. Han, D., et al.: A case study on common mode electromagnetic interference characteristics of GaN HEMT and Si MOSFET power converters for EV/HEVs. IEEE Trans. Transp. Electrif. 3(1), 168–179 (2016)
22. Zhong, Y., et al.: MMC with parallel-connected MOSFETs as an alternative to wide bandgap converters for LVDC distribution networks. J. Eng. 2017(5), 149–157 (2017)
23. Roscoe, N.M., et al.: LV converters: Improving efficiency and EMI using Si MOSFET MMC and experimentally exploring slowed switching. IEEE J. Emerging Sel. Top. Power Electron. 6(4), 2159–2172 (2018)
24. Rizzoli, G., et a.: Comparative experimental evaluation of zero-voltage-switching Si inverters and hard-switching Si and SiC inverters. IEEE J. Emerging Sel. Top. Power Electron. 7(1), 515–527 (2019)
25. Rezaei, M.A., Lee, K.-J., Huang, A.Q.: A high-efficiency flyback micro-inverter with a new adaptive snubber for photovoltaic applications. IEEE Trans. Power Electron. 31(1), 318–327 (2015)
26. Arab Ansari, S., et al.: Fault ride-through capability enhancement for microinverter applications. J. Renewable Energy 2019, 1–12 (2019)
27. Ansari, S.A., et al.: Comparative Evaluation of Si MOSFET-based Soft Switching DC-DC Converters and GaN HEMT-based Hard Switching DC-DC Converters. In: The 10th International Conference on Power Electronics, Machines and Drives (PEMD), Nottingham, the United Kingdom (2020)
28. Hart, D.W.: Power Electronics, 1st ed. McGraw-Hill Education, New York, USA (2011)
29. Ansari, S.A., Moghani, J.S.: A novel high voltage gain noncoupled inductor SEPIC converter. IEEE Trans. Ind. Electron. 66(9), 7099–7108 (2018)
30. Graovac, D., Purschel, M., Kiep, A.: MOSFET power losses calculation using the data-sheet parameters. Infineon Application Note 1.1 (2006)
31. Efthymiou, L., et al.: Zero reverse recovery in SiC and GaN Schottky diodes: A comparison. In: 2016 28th International Symposium on Power Semiconductor Devices and ICs (ISPSD), Prague, Czech Republic, pp. 71–74 (2016)
32. Micrometals: Iron powder cores for power conversion and line filter applications. Micrometals, February no. L (2007)
33. Thermal Materials. https://dm.henkel-dam.com/is/content/henkel/lt-8116-brochure-thermal-interface-materials-selection-guidepdf (2019)
34. Mouser Electronics. https://www.mouser.co.uk/
35. Anglialive. https://www.anglia-live.com/
36. Pace Components. http://www.pacecomponents.co.uk/

How to cite this article: Ansari SA, Davidson JN, Foster MP. Evaluation of silicon MOSFETs and GaN HEMTs in soft-switched and hard-switched DC-DC boost converters for domestic PV applications. *IET Power Electronics*. 2021;1–12. https://doi.org/10.1049/pel2.12085